Natural Ground Information Detection Method Based on GNSS Ground Reflection Delay Signal

Peigen Peng[#], Yongqi Li[#,*], Jian Zhao[#]

Department of Geospatial Information, Information Engineering University, Zhengzhou, Henan, 450000 China

#These authors contributed equally.

*Corresponding author: 1095997076@qq.com

Abstract: For natural surface disasters in key areas, if small deformations such as surface subsidence and displacement can be continuously monitored, it can provide early warning and effectively protect people's lives. In the past, small deformations were mainly measured by using GNSS direct signal to calculate displacement changes or by using SAR information, which can only measure one point. To monitor the deformation of an area, multiple monitoring points need to be deployed. Based on this, this paper mainly adopts GNSS ground reflection delay signal, and according to the different information of direct and reflection signal paths, combined with the geometry of receiver and ground reflection point and satellite, it can solve the small deformation of the ground surface, and realize the original point measurement to surface measurement while maintaining the original measurement accuracy, so as to improve the high-precision monitoring range and reduce the number of monitoring points.

Keywords: BeiDou; GNSS-R; Ground surface micro deformation monitoring.

1. Introduction

In recent years, underground resource exploitation and urban underground space construction are rapid, resulting in serious damage to the surface and internal structure of the ground, and geological disasters such as urban road subsidence and bridge collapse occur frequently[1].

If we can continuously monitor small deformations such as surface subsidence and displacement, we can guarantee people's lives effectively by providing early warning. Therefore, it is of great significance and value to carry out research on real-time, continuous and spatially covered large terrain deformation monitoring technology[2]. But at present, the monitoring of terrain is mainly for long-term observation, geological survey, deformation measurement and early warning of disaster-prone areas, traditional geodesy and photogrammetry are long-periodical, which is difficult to meet the demand of real-time monitoring, and is influenced by human factors, the personal safety of personnel working in disaster-prone areas will have a high risk, and when the disaster occurs, personnel can not quickly reach the scene for deformation measurement. It is difficult to provide timely feedback on the deformation information; and the monitored data is in a single form with low positioning accuracy, which makes it difficult to effectively monitor and warn the geological hazard potential sites in real time[3].

2. Model assumptions and notation

2.1 Notations

Important notations used in this paper are listed in Table 1.

Table 1 Notations

Symbols	Symbolic meaning
J	Navigation satellite number
I	I Branch Road
Q	Q-branch
A	Signal amplitude
C(t')	Pseudorandom code
f_c	Navigation signal carrier frequency
φ	Carrier Initial Phase
τ_{er}	Unknown time deviation between receiving and sending platforms
f_d	Doppler shift
f_1	IF frequency after demodulation of the navigation receiver
Δf_1	

3. Model construction and solving

3.1 High-resolution surface information extraction based on InSAR imaging

Since GNSS emits navigation radio waves, signal bandwidth, transmit power, etc. are not SAR signals specifically designed for high-resolution radar, thus there are many limitations in the precise detection of deformation[4].

As for the interferometry of SAR technology for the surface, the InSAR antenna is used to move along the radar body shifted long line array at equal speed on the surface to be measured, and radiates the phase reference signal, and the echoes received at different locations are processed coherently, so as to achieve high-resolution distance measurement and two-dimensional imaging at different measurement points.

For the resolution aspect of InSAR imaging, since it mainly depends on the distance-to-resolution and direction-to-resolution, which is related to the beam width, thus the detected SAR is analyzed using FM continuous wave, the coupled signal of continuous wave radar is analyzed, the radar band and signal waveform are obtained, and based on the constraints of microwave principal oscillation, digital frequency and signal under the phase reference coefficient, the digital elimination of the coupled signal is performed to reduce signal-to-noise ratio and improve the resolution of imaging[5].

The SAR system and terrain relationship model is matched with the radar image based on the geometric mapping of distance and direction in three dimensions, and the matching error of the radar image is corrected or analyzed in the direction of the main decision of the resolution, so as to obtain the high-precision information reflecting the surface morphology[6]. In addition, the SAR satellite has a short re-entry period, so the echo coherence processing can avoid the time decoherence and spatial decoherence caused by the long time span, thus achieving the high-resolution acquisition of surface information. Schematic diagram of InSAR imaging process is shown in Figure 1.

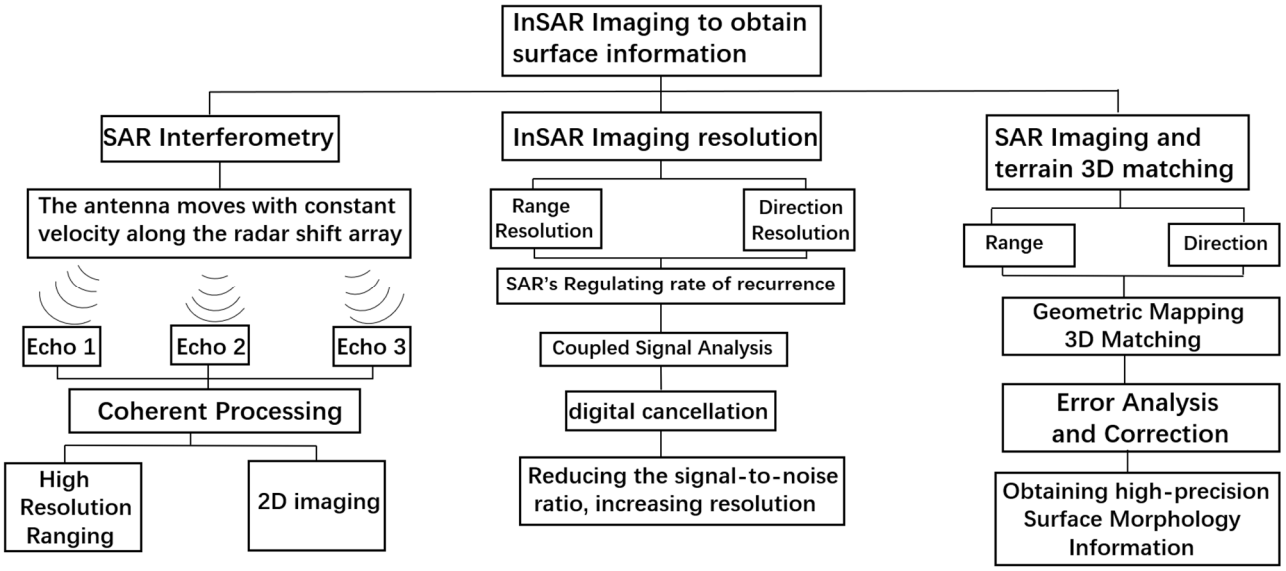


Figure 1 Schematic diagram of InSAR imaging process

3.2 BDS satellite based dual base SAR signal model

3.2.1 Transmit signal model

The carrier signal and navigation data are transmitted at the B3 frequency point of the BDS. Since the transmitting process carries out pseudo-random code spreading of the signal at a code rate of 10.23 MHz as well as orthogonal phase shift modulation of the carrier, and synchronous modulation of the spreading code and navigation information is achieved by mode two and, then the B3 frequency point signal is carried out by orthogonal modulation of two branches on the carrier can be expressed as the BDS multi-frequency combined navigation signal consists of a pseudo-random code orthogonal to the navigation data on the carrier, and its calculation can be expressed as.

$$S^{j}\left(t^{'}\right)=A_{I}C_{I}^{j}\left(t^{'}\right)D_{I}^{j}\left(t^{'}\right)\cos\left(2\pi f_{c}t^{'}+\varphi^{j}\right)+A_{Q}C_{Q}^{j}\left(t^{'}\right)D_{Q}^{j}\left(t^{'}\right)\sin\left(2\pi f_{c}t^{'}+\varphi^{j}\right) \tag{1}$$

where I and Q represent the two branches, C(t`) is the C/A code, D(t`) is the modulated navigation data on the spread spectrum code, and fc is the carrier frequency.

For simplicity of calculation only one way signal can be considered, if the signal amplitude and satellite number are omitted, the above equation can be simplified as.

$$S\left(t^{'}\right)=C\left(t^{'}\right)D\left(t^{'}\right)\cos\left(2\pi f_{c}t^{'}\right) \tag{2}$$

3.2.2 Receiving signal model

Direct wave signal.

$$S_{D}\left(t^{'}\right)=S\left(t^{'}-\tau_{D}\left(t^{'}\right)\right) \tag{3}$$

Among them

$$\tau_{D}\left(t^{'}\right)=\frac{\left|\mathbf{P}_{S}\left(t^{'}\right)-\mathbf{P}_{D}\right|}{c}$$

denotes the delay caused by the direct wave propagation path at moment t`.

Echo signal.

$$S_{R}\left(t^{'}\right)=\sigma_{T}S\left(t^{'}-\tau_{R}\left(t^{'}\right)\right) \tag{4}$$

τ R(t') can be expressed as.

$$\tau_{R}\left(t^{'}\right)=\frac{\left|\mathbf{P}_{S}\left(t^{'}\right)-\mathbf{P}_{T}\right|+\left|\mathbf{P}_{T}-\mathbf{P}_{R}\right|}{c}$$

is the delay caused by the echo propagation path at the moment t`.

According to the principle of SAR signal processing, the above one-dimensional signal needs to be converted into two-dimensional signal. Combined with the BDS pseudo-random code period of

1ms, the PRT can be 1ms for two-dimensional segmentation of the data by distance to time t and direction to time u. And the direct wave signal after demodulation by the receiver IF is.

$$\begin{aligned} S_D(t,u) &= C\left(t-\tau_{err}-\tau_D(u)\right)\exp\begin{pmatrix} -j2\pi f_c\tau_D(u) - j2\pi f_c\tau_{err} \\ -j2\pi\left(f_d+f_I\right)t - j2\pi\Delta f_I u \end{pmatrix} \\ &= C\left(t-\tau_{err}-\frac{\left|\mathbf{P}_s(u)-\mathbf{P}_D\right|}{c}\right)\exp\begin{pmatrix} -j2\pi f_c\dfrac{\left|\mathbf{P}_s(u)-\mathbf{P}_D\right|}{c} \\ -j2\pi f_c\tau_{err} - j2\pi\left(f_d+f_I\right)t \\ -j2\pi\Delta f_I u \end{pmatrix} \end{aligned} \tag{5}$$

Similarly, the echo signal can be expressed as.

$$\begin{aligned} S_R(t,u) &= \sigma_T\cdot C\left(t-\tau_{err}-\tau_R(u)\right)\exp\begin{pmatrix} -j2\pi f_c\tau_R(u) - j2\pi f_c\tau_{err} \\ -j2\pi\left(f_d+f_I\right)t - j2\pi\Delta f_I u \end{pmatrix} \\ &= \sigma_T\cdot C\left(t-\tau_{err}-\frac{\left|\mathbf{P}_S(u)-\mathbf{P}_T\right|+\left|\mathbf{P}_T-\mathbf{P}_R\right|}{c}\right) \end{aligned} \tag{6}$$

3.3 Analysis of BDS-based dual-base SAR inverse projection imaging processing

3.3.1 Direct wave capture tracking

The determination of the transmitting source satellite is achieved by roughly estimating the carrier frequency and the pseudo-random code phase based on the capture of the direct wave signal[7].

Due to the Doppler shift generated by the relative motion of the SAR satellite and the Earth, the deviation of the nominal satellite frequency from the IF frequency needs to be determined to reduce the signal-to-noise ratio of the radar system and the attenuation of the distance-to-resolution[8].

Based on the fuzzy function, the signal with frequency shift is matched and filtered, and the peak amplitude of the output decreases rapidly with the increase of frequency deviation due to the high correlation between the two, as shown in Figure 2.

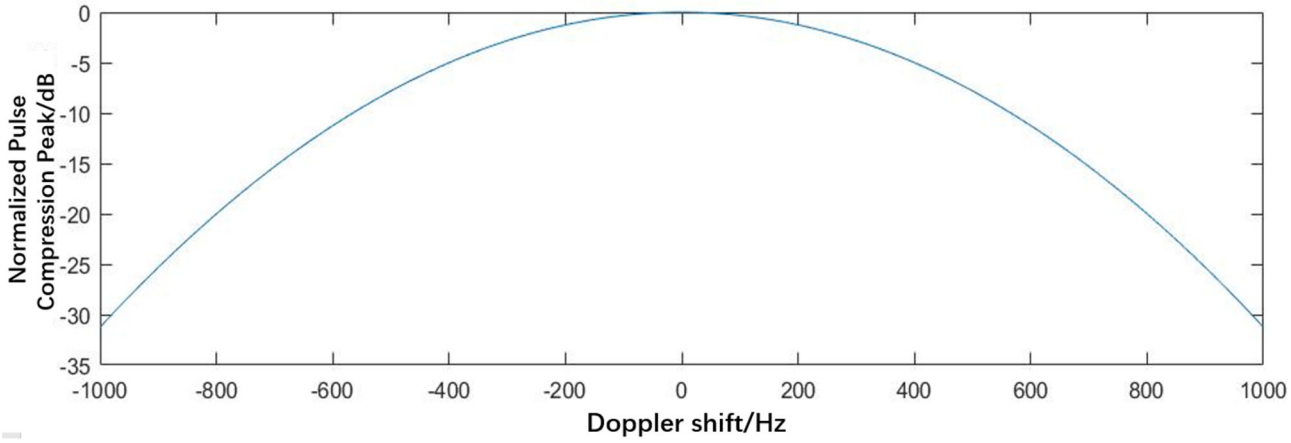


Figure 2 Sensitivity of pseudorandom codes to Doppler frequency bias

At the starting moment of capturing the navigation signal, the Doppler frequency and code phase are uncertain, but by traversing the loop to calculate all the possible values of both, the maximum value of the relevant operation is found, which is the corresponding rough value of Doppler frequency shift and code phase to achieve the purpose of capturing the rough value.

However, after the rough value is obtained and the coarse synchronization is achieved, the carrier frequency is continuously shifted due to the Doppler effect caused by the continuous motion of the satellite, and the pseudo-random code phase also changes with the change of the distance between the satellite and the receiver, so the navigation signal needs to be dynamically tracked to ensure the continuous and stable Doppler shift and navigation message. Thus, the local carrier and the received

carrier can be more accurately synchronized to reduce errors and to improve the correlation between the pseudorandom code of the receiver and the pseudorandom code in the received navigation signal.

Specifically, the correlation between the input signal and the three locally generated pseudo-random codes is calculated as follows.

The results of the ahead branch (E), immediate branch (P) and lagging branch (L) are multiplied and then integrated and accumulated to obtain the correlation between the local and received pseudorandom codes, and then the theoretical IF value is used as feedback to adjust the phase of the local pseudorandom codes. By the above process the direct wave signal can be expressed as.

$$S_D(t,u) = C\left(t - \tau_{err} - \frac{\left|\mathbf{P}_S(u) - \mathbf{P}_D\right|}{c}\right)\exp\begin{pmatrix} -j2\pi f_c \dfrac{\left|\mathbf{P}_S(u) - \mathbf{P}_D\right|}{c} \\ -j2\pi f_c \tau_{err} - j2\pi \Delta f_I u \end{pmatrix} \tag{7}$$

Similarly, the echo signal can be expressed as.

$$S_R(t,u) = \sigma_T \cdot C\left(t - \tau_{err} - \frac{\left|\mathbf{P}_S(u) - \mathbf{P}_T\right| + \left|\mathbf{P}_T - \mathbf{P}_R\right|}{c}\right) \tag{8}$$

$$\exp\begin{pmatrix} -j2\pi f_c \dfrac{\left|\mathbf{P}_S(u) - \mathbf{P}_T\right| + \left|\mathbf{P}_T - \mathbf{P}_R\right|}{c} \\ -j2\pi f_c \tau_{err} - j2\pi \Delta f_I u \end{pmatrix}$$

The direct wave is captured and tracked to complete the decoding operation of the navigation message, and then the spatial position information of the corresponding navigation satellite at the time of the navigation signal transmission is obtained.

3.3.2 Dual Base SAR Time-Frequency Synchronization

The received direct signal is compressed with PRT pulse, and the corresponding navigation satellite standard C/A code is used as the reference signal to extract the azimuthal peak position, which is used as the standard for the two-dimensional differentiation of the direct and echo signals for time synchronization and calibration[9].

The direct wave signal after time synchronization and the local pseudo-random code do the distance-oriented pulse processing, which can be expressed as.

$$S_D(t,u) = p_{CA}(t)\exp\begin{pmatrix} -j2\pi f_c \dfrac{\left|\mathbf{P}_S(u) - \mathbf{P}_D\right|}{c} \\ -j2\pi f_c \tau_{err} - j2\pi \Delta f_I u \end{pmatrix} \tag{9}$$

Where, PCA is the result of the signal after time synchronization with the standard C/A code inter-correlation.

Similarly, the echo signal can be expressed as.

$$S_R(t,u) = \sigma_T \cdot p_{CA}\left(t - \frac{\left|\mathbf{P}_S(u) - \mathbf{P}_T\right| + \left|\mathbf{P}_T - \mathbf{P}_R\right| - \left|\mathbf{P}_S(u) - \mathbf{P}_D\right|}{c}\right) \tag{10}$$

$$\cdot\exp\begin{pmatrix} -j2\pi f_c \dfrac{\left|\mathbf{P}_S(u) - \mathbf{P}_T\right| + \left|\mathbf{P}_T - \mathbf{P}_R\right|}{c} \\ -j2\pi f_c \tau_{er} - j2\pi \Delta f_I u \end{pmatrix} \tag{11}$$

Extract the direct wave signal distance to the pulse compression peak phase, remove this item in the echo term pulse compression results, that is, to achieve frequency synchronization, to obtain the echo signal.

$$S_R(t,u) = \sigma_T \cdot p_{CA}\left(t - \frac{\left|\mathbf{P}_S(u) - \mathbf{P}_T\right| + \left|\mathbf{P}_T - \mathbf{P}_R\right| - \left|\mathbf{P}_S(u) - \mathbf{P}_D\right|}{c}\right) \tag{12}$$

$$\cdot \exp\left(-j2\pi f_c \frac{\left|\mathbf{P}_S(u)-\mathbf{P}_T\right|+\left|\mathbf{P}_T-\mathbf{P}_R\right|-\left|\mathbf{P}_S(u)-\mathbf{P}_D\right|}{c} \right) \tag{13}$$

3.3.3 Echo Focus

Finally, the inverse projection imaging of the scene echo signal is completed in the time domain. In the first step, a planar grid is divided in the target scene area, after which the coordinates (xi,yi) of each point on each grid point under each sampling moment in each azimuthal direction to the sum of the two-station slant distances from the navigation satellite to the echo receiving antenna and to the direct antenna, respectively[10], are (|Ps(μ)-PT|+|PT-PR|) and (|Ps(μ)-PD|), which are used to form the phase compensation factor, while The satellite position vector PS(μ) at each azimuthal sampling moment has been derived by decoding the navigation message, so the dual-base synthetic aperture radar reverse projection imaging can be expressed as.

$$\begin{aligned} I\left(x_i,y_j\right)=\sum_u \Bigg[& \sigma_T \cdot p_{CA}\left(t-\frac{\left|\mathbf{P}_S(u)-\mathbf{P}_T\right|+\left|\mathbf{P}_T-\mathbf{P}_R\right|-\left|\mathbf{P}_S(u)-\mathbf{P}_D\right|}{c} \right) \\ & \cdot \exp\left(-j2\pi f_c \frac{\left|\mathbf{P}_S(u)-\mathbf{P}_T\right|+\left|\mathbf{P}_T-\mathbf{P}_R\right|-\left|\mathbf{P}_S(u)-\mathbf{P}_D\right|}{c} \right) \\ & \cdot \exp\left(j2\pi f_c \frac{\left|\mathbf{P}_S(u)-\mathbf{P}_{x,y_j}\right|+\left|\mathbf{P}_{x_i,y_j}-\mathbf{P}_R\right|-\left|\mathbf{P}_S(u)-\mathbf{P}_D\right|}{c} \right) \Bigg] \end{aligned} \tag{14}$$

4. Conclusion

In this paper, the GNSS ground reflection delay signal is mainly used. According to the different information of the direct and reflected signal paths, combined with the geometry of the receiver, the ground reflection point and the satellite, the small deformation of the ground surface is calculated, and the original measurement accuracy is maintained. From the original point measurement to the surface measurement, the high-precision monitoring range is improved and the number of monitoring points is reduced. From this method, it can be seen that if the target is located exactly on the grid division point, the phase difference caused by the transmission path can completely cancel thus achieving the maximum signal-to-noise ratio; while for the target located between the grid points, the signal-to-noise ratio is relatively lower.

References

[1] Li Z.P. Application of GNSS surface deformation monitoring and internal tilt monitoring in landslide deformation monitoring [J]. Western Transportation Science and Technology, 2021, 32-35.

[2] Jiang L. Analysis of GNSS-based slope deformation monitoring method for open pit mines [J]. Electronic Technology and Software Engineering,2022, 243-246.

[3] Zhao Wenhao. Real-time data communication and decoding of GNSS landslide deformation monitoring system [C]. Nanchang, Jiangxi: Proceedings of the 12th Annual China Satellite Navigation Conference - S01 Satellite Navigation Industry Applications,2021:13-18.

[4] Tang Z. Interferometric synthetic aperture radar - a powerful tool to realize "digital earth"[J]. Aviation Knowledge,2005(01):18-22.

[5] Zhao ZW. Satellite Scanning Interference Synthetic Aperture Radar System and Signal Processing Technology[D]. Beijing:Graduate School of Chinese Academy of Sciences(Institute of Electronics),2007,51-73.

[6] Xue, H. W. Interferometric synthetic aperture radar measurement of some key technologies[D]. Xi'an:Xi'an University of Electronic Science and Technology,2017,88-94.

[7] Liu Baoquan. Research on key technologies of interferometric synthetic aperture radar measurement[D]. Xi'an:Xi'an University of Electronic Science and Technology,2008,98-123

[8] Wang, Y., Jiang, Y. S.. Star-star synthetic aperture imaging system for BeiDou satellite backscattered signals: concept and feasibility[J]. Journal of Radar,2012(02):18-33.

[9] Zhang T. Research on dual-base differential interference SAR deformation inversion based on navigation satellites[D]. Beijing:Beijing University of Technology,2017,133-156.

[10] Han Junqiang. Research on high precision GNSS real-time landslide deformation monitoring technology and environmental modeling analysis[J]. Journal of Surveying and Mapping, 2020,22-29.